ALKALI SILICA REACTION IN MORTARS MADE FROM AGGREGATES HAVING DIFFERENT DEGREES OF CRYSTALLINITY

ANA MLADENOVIČ, SAŠO ŠTURM*, BREDA MIRTIČ**, JERNEJA STRUPI ŠUPUT

Slovenian National Building and Civil Engineering Institute,
Dimičeva 12, 1000 Ljubljana, Slovenia
**Jožef Stefan Institute, Department for Nanostructured Materials,*
Jamova 39, 1000 Ljubljana, Slovenia
*** Faculty of Natural Sciences and Engineering, Department of Geology,*
University of Ljubljana, Aškerčeva 12, 1000 Ljubljana, Slovenia

E-mail: ana.mladenovic@zag.si

Submitted March 8, 2008; accepted November 24, 2008

Keywords: Alkali-silica reaction, Aggregates, Linear expansion, SEM, EDS

In the study, mortar bars containing three different types of silica aggregate and aged according to ASTM C 1260 were examined in order to investigate the characteristics of the reaction rims which occur between individual grains of these aggregates and the cement paste due to alkali-silica reaction (ASR). Three silica aggregates were used: well-crystalline quartz crystal, intermediate-crystalline flint, and poorly-crystalline diatomite. SEM was used to determine the morphology of the reaction rims, and EDS to determine their chemical composition. The quantity of Si ions diffusing towards the cement paste was determined, as well as the quantity of Ca ions and alkalis diffusing towards the silica aggregate. It was found that, in the case of the flint aggregate, the $CaO–SiO_2$ rich gel caused, after 18 days of ageing, a linear expansion of approximately 0.24 %, whereas in the case of the diatomite aggregate, an expansion of approximately 0.56 % was observed (no significant expansion occurred in the case of the quartz aggregate). It was found that alkali silica reaction correlates inversely with crystallinity, although a strong effect was observed in the case of the intermediate- and poorly-crystalline aggregates, which, at certain volume proportions in concrete and mortar, could predominate over the effect of crystallinity.

INTRODUCTION

Alkali-silicate reaction (ASR) is a pathogenic reaction in cement composites, which is caused by the attack of alkalis and hydroxyl groups on certain siliceous rocks and minerals found in aggregates. This reaction product is a hydrophyllic gel, which expands and applies pressure to the surrounding concrete. Characteristic cracks occur, and reaction products are deposited on the surface. Such cracks are dangerous since it is then possible for water can penetrate into the body of the concrete, and accelerate degradation. For this reason the expansion of concrete and mortar due to alkali-silica reaction (ASR) has been extensively investigated.

It is well known that the degree of crystallinity of silica aggregate is one of the major factors influencing alkali reactivity. Poorly-crystallized polymorphs of silica have higher Gibbs free energies and are thus thermodynamically less stable than well-crystallized species, which means that reactivity decreases over the range from amorphous to well-crystallized species of silica [1]. This has been confirmed by results obtained by numerous authors [2, 3, 4]. Amorphous species (opal-A, volcanic glass) consist of irregular arrangements of SiO_4 frameworks, and do not contain much bridging oxygen. They frequently contain water as well as micropores between the structural units. The poorly-crystalline species (opal-CT, cristobalite, tridymite) have a very open structure containing channels through which relatively large ions can pass, as well as numerous dislocations and imperfections [5]. These properties increase the solubility of such material. On the other hand, well-crystalline species (quartz), have well-arranged, defect-free crystal lattices, which are less sensitive to dissolution [6].

A frequently used method for determining the crystallinity of minerals and silica-containing rocks is the crystallinity index (CI) method according to Murata and Norman [7]. They defined the crystallinity index of quartz, based on the sharpness of the quintuplet which occurs between 67° and 69°. However, it is not known which type of structural disorder in the crystal lattice is responsible for the deterioration of the supposedly ideal crystallinity index of 10. Using this method, Katayama et al [8] and Katayama [9] found that siliceous materials tend to recrystallize through diagenesis, metamorphosis and alteration, from an amorphous-opaline state through an intermediate fine-grained mixture of chalcedony and microcrystalline quartz, to a final coarse mosaic of granular quartz. This is paralleled by a corresponding increase in the crystallinity index as determined by XRD.

It is also interesting to note that Morino [10] found a close connection between the reactivity and crystallinity indices of different cherts, which had values in the range between 3.92 in 7.14.

However, opinions vary about the nature of the reaction mechanism itself. Different theories have been developed, and different types of aggregate have been used in the studies. According to Powers and Steinour [11], alkali-silica gel is expansive, whereas lime–alkali–silica gel is non-expansive. This theory was later supported, though in a slightly modified form, by Wang and Gillot [12]. They determined that a maximum concentration of alkalis occurred in the middle part of the reaction rim between the investigated opal aggregate and the cement paste. They also found that the concentration of Ca decreased exponentially in the direction from the cement paste towards the silica aggregate. Chatterji [13], however, contended, contrary to the opinion of the above-mentioned authors, that lime–alkali–silica gel, as well alkali–silica gel, is expansive. The results of his research showed that hydroxide attacks on silica grains are always accompanied by the penetration of potassium, sodium and calcium cations to reaction sites.

As is well known, the speed of diffusion of ions is governed by several factors, such as their diameter, charge, and local differences in potential. The interaction of ions with water, i.e. their hydration, further restricts the speed of diffusion. The Ca^{2+} ions are smaller than the K^+ and Na^+ ions, and also have higher charges and have higher polarization energies. When hydrated, however, the Ca^{2+} ions become bigger than the K^+ and Na^+ ions [14, 15, 16]. This explains why, in accordance with the Stokes-Einstein relation for the diffusion coefficient, which predicts that the smaller the particle the more mobile it tends to be, the monovalent K and Na ions penetrate the pores at a faster rate than the calcium ions.

According to Chatterji [13], the rate of diffusion of silica ions from the grains, as well as the rate of penetration of the alkali ions towards the grains, is determined by the concentration of calcium ions in the vicinity of the grain. Expansion of the grain occurs when more material enters it than leaves it. Using transmission electron microscopy on artificially aged mortar bars, Groves and Zhang [17] found lime-alkali-silica gels with a Ca/Si ratio of approximately 1.0, and considered that gel of this kind was responsible for the expansion of the investigated mortar bars. Brouxel [18] additionally found that, in the case of concretes aged under natural conditions, in the part of the reaction rim where the alkali concentration was at its maximum the Ca/Si ratio is 1.0, and that the amount of silica decreased exponentially in the direction from the silica aggregate towards the cement paste. In the concrete specimens which he examined, Brouxel found only lime-alkali-silica gels. He did not find any pure alkali-silica gels, which, according to Powers and Steinour, are alone responsible for expansion. However, while not agreeing with the Wang and Gillot theory, Brouxel considered that the part of the gel with the highest content of alkalis is probably the part which is the most susceptible to water. Similar findings about the expansive properties of lime–alkali–silica gels have been reported by several authors [19, 20, 21]. A third theory about the alkali-silica mechanism has been recently postulated by Prezzi et al. [22], who proposed a model based on the Gouy-Chapman double-layer theory in order to explain the expansion caused by alkali–silica reaction in concrete. According to this theory, ions with higher valencies result in a thinner double layer of ions, causing comparatively smaller gel expansion. The greater the concentration of the bivalent calcium ions relative to the monovalent sodium and potassium ions, the smaller is the expansion in the concrete.

The morphology and chemical composition of laboratory gels and gels obtained from field examinations of concrete structures have been analysed by numerous researchers [21, 23, 24, 25, 26, 27, 28, 29], who have found that many differently crystallized forms of reaction products occur apart from the most frequently observed amorphous gels. These reaction products have varying composition and appearance, depending on their location in the concrete or mortar. According to Laing et al. [30], there does not appear to be a complete solid solution between the alkali lime silica gel and C–S–H gel, although some researchers, e.g. [31], consider that gels in deteriorated concretes have a continuous range of composition, from typical cement hydrates to typical ASR gels. The following general trends have been observed in reaction rims, in the direction from the reactive aggregate to the cement paste: (1) a rapid decrease in the SiO_2 content at the aggregate contact, followed by a slow decrease, (2) a rapid increase in the CaO content at the aggregate contact, followed by a slow decrease, (3) a maximum alkali content approximately in the middle of the reaction rim, followed by a slow decrease.

In order to improve our general understanding of the mechanism of alkali–silica reaction with respect to the mineralogical type and crystallinity of silica aggregates, while at the same time taking into account known findings from the literature, it was decided to investigate these two effects by measuring the expansion of mortar bars made using three different types of aggregate aged under accelerated laboratory conditions, as well as by investigating the chemical composition of the gel in the reaction rims, and the distribution of individual chemical elements inside these rims. The three different types of silica aggregate used in the investigation were: (1) quartz crystals with the highest degree of crystallinity, which were considered to be non-reactive with regard to alkali-silica reactivity, (2) flint, as an example of intermediate crystallinity and reactivity, and (3) diatomite, as an example of an aggregate having poor crystallinity but a high level of alkali-silica reactivity.

EXPERIMENTAL

Aggregate

The three aggregates selected for the preparation of the mortar bars were: (1) hydrothermal quartz crystals from Znojile in central Slovenia, (2) optically dense, non-porous biogenic flint of Upper Triassic age from Jersovec in north-east Slovenia, and (3) dense diatomite from Spančevo Kočani, in Macedonia. Their average chemical compositions, as determined by EDS analysis, are presented in Table 1.

The mineralogical compositions of the investigated aggregates, as shown in Table 2, were determined by X-ray powder diffractometry using a Philips PW 3710 diffractometer and CuKα radiation, a Ni filter and a graphite monochromator by scanning the interval 2θ = 5-70°. The scanning rate was 1°/min except for the range 2θ = 66° – 69°, where scanning was performed at the slower rate of 0.25 °/min in order to determine the crystallinity index (CI) of the aggregates. The selected quartz crystal was used as a standard sample, and a CI value of 10 was allocated to this sample. The accuracy of scanning was ± 0.02°. Determination of the grain size of the quartz in the investigated aggregates, as well as the identification of chalcedony, was performed by means of optical microscopy in transmitted polarized light.

Table 1. Average chemical composition of the selected aggregates.

Oxide (wt. %)	Quartz crystal Q	Flint F	Diatomite D	Inert quartz sand IA
SiO_2	99.69	95.06	96.46	93.07
Al_2O_3	0.08	1.59	1.30	3.61
Fe_2O_3	-	1.50	1.76	-
CaO	-	1.01	0.01	-
Na_2O	0.09	-	-	2.06
K_2O	-	0.71	-	1.26

Table 2. Mineralogical composition of the selected aggregates, together with the CI index of the quartz in these aggregates.

Aggregate	Mineralogical composition	CI index
Quartz crystal	quartz	10.0
Flint	cryptocrystalline quartz, chalcedony, with traces of calcite, chlorite and illite	5.8
Diatomite	opal CT [32] with cryptocrystalline quartz	< 1.0

Mortar bars

In order to study the alkali-silica reaction which occurs when the above-described aggregates are used, a series of mortar bars (3 test specimens for each aggregate) were prepared for the accelerated test in accordance with the requirements of the standard ASTM C 1260. Since it is well-known that poorly-crystalline and, therefore, strongly reactive silica polymorphs, such as flint and diatomite, usually show a pessimum effect (Ozol, 1975; Hobbs, 1978), these two aggregates were investigated both in pure form (100 % aggregate) and in the form of mixtures made from the aggregate and normalized quartz sand according to EN 196-1 (manufacturer: Normensand, Germany), using a by-weight ratio of 5.0 % aggregate and 95.0 % inert sand. Thus the total number of investigated mortar bars was 15. They differed only with respect to the type and amount of reactive silica aggregate which they contained. In all the experiments Portland cement designated CEM I 42.5 R according to EN 197-1, and having an alkali content of 0.85 % determined as the Na_2O equivalent, was used. A summary of data on the mortar bar sets is given in Table 3.

After the accelerated mortar bar tests had been performed, the quantity, chemical composition and morphology of the gels and the manner of dissolving of the aggregate grains were investigated by analysing dry mortar samples. Fractured mortar bars and polished thin-sections of mortar bars were prepared and studied by using a conventional tungsten-cathode SEM (JEOL, JSM 5800) equipped with with a detector of back-scattered electrons (BSE) and an EDS analytical system (Link ISIS-300). In order to prevent charging, the surfaces of the samples were first coated with a film of carbon approximately 20 nm thick. They were then examined in back-scattered electrons (BSE), which are sensitive to differences in chemical composition, at standardized SEM working conditions with regard to accelerating voltage, working distance and electron beam current. Quantitative EDS analysis (spot and line profiles) was performed on the polished thin sections and fractured samples of the mortar bars, applying the internal standards stored in the Link ISIS-300 data library. Each analysis lasted 60 seconds.

The morphology and chemical composition of the gels was analysed at several locations on the polished thin

Table 3. Composition and w/c ratio of the investigated mortar bar sets.

Bar set designation	Aggregate content in grams				Active/inert aggregate ratio (%)	Cement content in grams	W/C ratio
	Quartz	Flint	Diatomite	Inert aggregate			
Q	990	–	–	–	100 : 0	440	0.47
F	–	990	–	–	100 : 0	440	0.47
F + IA	–	49.5	–	940.5	5 : 95	440	0.47
D	–	–	990	–	100 : 0	440	0.47
D + IA	–	–	49.5	940.5	5 : 95	440	0.47

sections and fractured surfaces of the individual mortar bars. It is well known that the results of such analyses are much more accurate when obtained on polished thin sections than those which can be obtained on fractured surfaces. Apart from this, specimens prepared in this way are much more representative for studying the manner of dissolution of aggregate grains. In order to limit, as far as possible, any changes in the composition of the analysed gels (i.e. any loss of alkalis), the thin sections were prepared using alcohol and not water (this was suggested by Regourd-Moranville (1989)). It was found that the differences in the chemical composition of the gels, as observed on the polished thin sections and the fractured surfaces, were very small, and smaller than those observed within the various different individual morphological types of gel from the same sample. In general, only an insignificant loss of alkalis was observed when the thin sections were prepared.

RESULTS AND DISCUSSION

Mortar bar expansion measurements

The results of measurements of the average linear expansion of the mortar bars, determined according to the ASTM C 1260 method, are presented in Figure 1. From this figure it can be seen that, as could be expected, the maximum average expansion occurred in the mortar bar sets F+IA and D+IA, made from 5 % aggregate and 95 % inert material (see Table 3). Maximum expansion, measured at the end of the exposure period, amounted to 0.239 % (flint) and 0.560 % (diatomite). In both cases, at the end of this period fine cracks and gel spots were observed on the surfaces of the specimens. This means that such a proportion of flint or diatomite in mixtures with a non-reactive aggregate should be considered to be extremely reactive, which at the same time means that, in the case of these two types of aggregate, a pessimum exists. Low, non-deleterious expansion, without the appearance of any cracks and/or signs of ASR, was observed in the other three mortar bar sets (Q – quartz crystal: 0.115 %, F - 100 % flint: 0.113 %, and D - 100 % diatomite: 0.106 %). Taking into account the pessimum effect, the expansion of mortar bars from an individual type of aggregate shows a negative correlation with the degree of crystallinity, defined in terms of the crystallinity index CI.

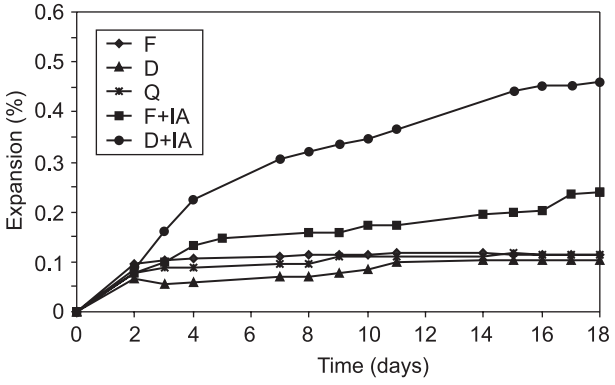

Figure 1. Average linear expansion of the investigated mortar bars.

SEM-EDS analysis

The average chemical composition and morphology of the reactive products was studied by SEM-EDS analysis on the polished thin-sections and on fractured samples of the five different types of mortar bars. The results of the analyses of the chemical composition of the reactive products are given for the polished thin sections in Table 4, the presented figures being in each case the average result of at least 20 measurements. It can be seen that all five investigated types of mortar bar contained lime-alkali-silica gels, consisting mainly of CaO and SiO_2, together with small amounts of Na_2O and K_2O. The CaO/SiO_2 ratio varied between 0.3 and 1.6. No pure alkali-silica gels were observed. The chemical composition of the gels varied to some extent not only from sample to sample, but also from location to location inside any particular sample. A detailed description of the morphology and chemical composition of the ASR products in the mortar bars with different silica aggregates is given in the following sections.

Quartz crystal aggregate (Q)

Figure 2 shows a BSE image of the mortar with the quartz crystal aggregate. Quartz particles having sharp edges (the result of the fact that these grains were produced by fracturing along the crystal cleavage) can be seen inside the mortar matrix.

Table 4. Average chemical composition of the observed gels (wt.%).

Aggregate	CaO	SiO_2	CaO/SiO_2	Na_2O	K_2O	Al_2O_3	SO_3
Q	56.62	41.63	1.36	0.17*	0.35	0.33	0.90
F	25.23	72.16	0.35	3.55	0.36	1.35	0.00*
F + IA	56.62	36.45	1.55	3.17	2.03	0.42*	1.32
D	43.56	54.28	0.80	0.05*	0.01*	1.18	0.92
D + IA	36.56	58.13	0.63	2.01	2.59	0.25	0.47

** The stated concentration is less than the standard deviation of the peak intensity (<2σ)*

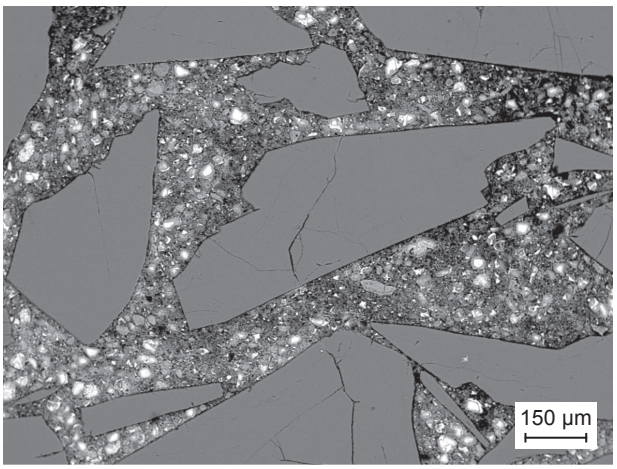

Figure 2. BSE image of single quartz crystal aggregate particles.

A more detailed investigation of this mortar revealed (see Figure 3a) a small amount of lime-alkali-silica gel, attached to a quartz particle. This gel was in the form of an amorphous layer, a few micrometres thick. At two locations cracks can be seen in the layer of gel, which are a result of dehydration during sample preparation. From the corresponding EDS spectrum shown in Figure 3b it can be seen that small quantities of Na_2O (1.42 %) and K_2O (0.45 %) are incorporated in the gel, for which reason it has been concluded that it was not a typical C–S–H gel.

As a result of the formation of lime–alkali–silica gel, dissolution of the quartz aggregate has occurred in the direction from the outside towards the interior of the grain, as has also been described by Lehman and Holzer (2003). This phenomenon can be seen in the BSE

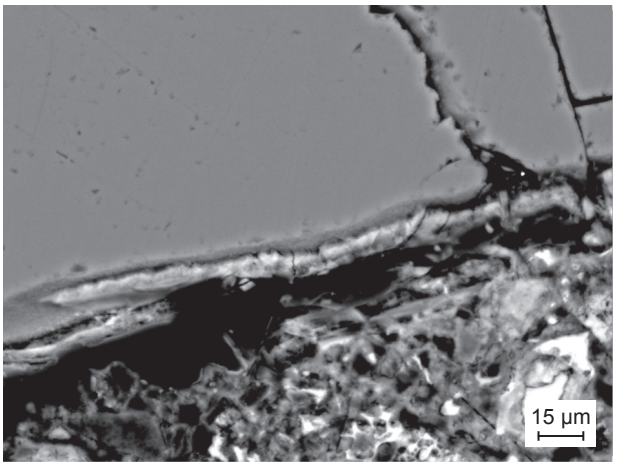

a)

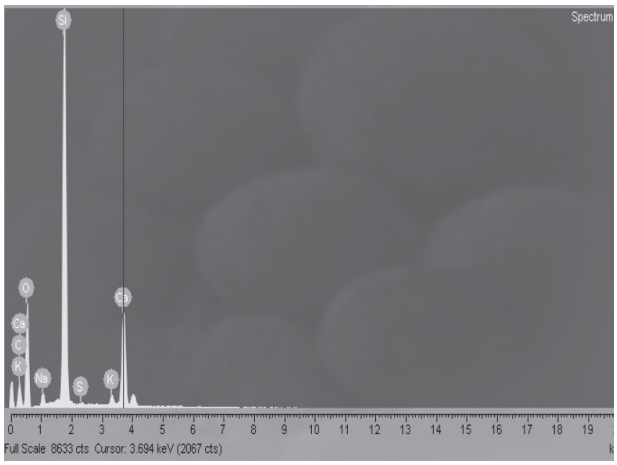

b)

Figure 3. (a) BSE image of a quartz aggregate particle with alkali-silica gel located along its edge (the cracks in the gel are marked by arrows); (b) EDS spectrum of the gel.

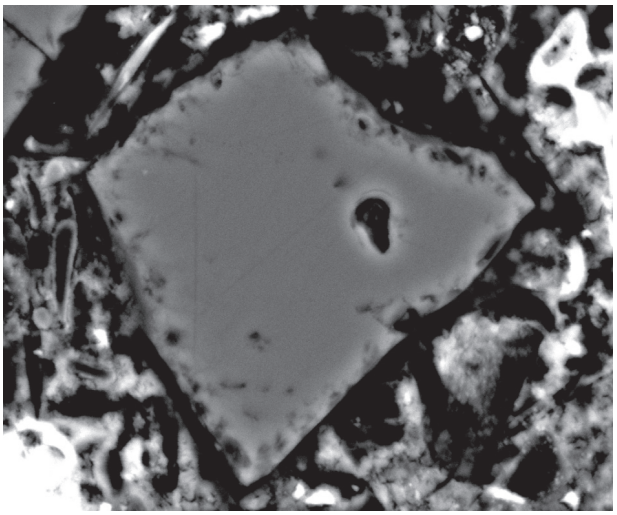

a)

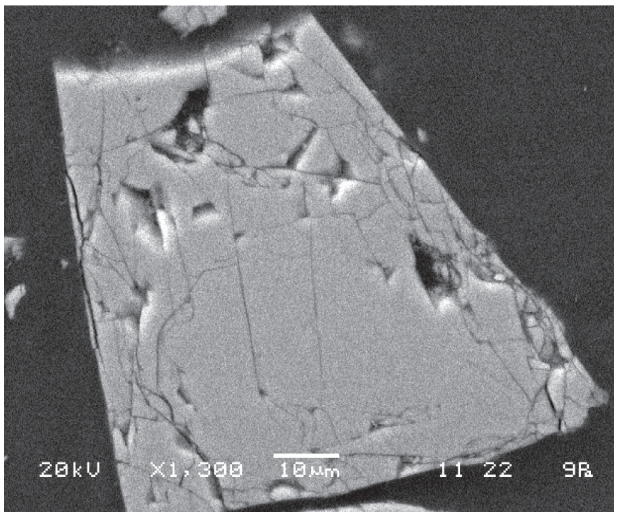

b)

Figure 4. (a) BSE image of a quartz aggregate particle damaged by alkaline attack; (b) for comparison, some grains of the fresh quartz aggregate.

image shown in Figure 4a, where the outer, brighter region of the damaged surface of the particle indicates partial dissolving of the SiO_2 matrix. For comparison, some grains of the fresh quartz aggregate are shown in Figure 4b, where it can be seen that the grains are cracked but have sharp, straight edges. It should be noted that crystalline (sponge-like) lime–alkali–silica gels, usually covering the surface of the quartz particles as a superficial, mould-like layer, were observed, in addition to the predominant amorphous lime–alkali–silica gels.

Flint aggregate (F, F+IA)

Compared to the sample of quartz aggregate, the lime–alkali–silica gels observed in the mortar bars containing pure flint aggregate (designated F) were similar in their features but occurred in larger quantities, which were often located as far as 500 μm from the aggregate particles, inside the paste and usually concentrated in air voids and microcracks. Figure 5a shows a cross-section of such an air void in the aggregate (F), which was lined with a thin layer of amorphous gel. The EDS spectrum of this gel is shown in Figure 5b. Due to dehydration in the sample preparation, the lime–alkali–silica gel inside the air void usually cracks and breaks into separate flake-like particles.

An example of fresh flint particles are shown in Figure 6a and 6b, and how a flint particles typically dissolve along the subgrain boundaries due to alkaline attack is shown in Figure 6c, and enlarged in Figure 6d. On the other hand, little damage can be observed on the surfaces of the subgrains, which suggests non-uniform composition of the flint particles. This indicates that the silica cement binding the subgrains dissolves more readily than the subgrains themselves (a similar characteristic dissolving mechanism has been observed on some sandstones which were investigated by Broekmans and Jansen [37], and by Rivard et al. [38]. The characteristic reaction products on the fractured surface of this sample are shown in Figures 7a and 7b, and the corresponding EDS spectrum is shown in Figure 7c.

A dramatic change in the microstructure was observed in the mortar made with F+IA aggregate, consisting of 5 % flint and 95 % inert aggregate, where a large amount of lime–alkali–silica gel formed next to the aggregate particles, as well as in microcracks and air voids. A BSE image of an air void lined with lime–alkali–silica gel, showing cracks in the gel due to dehydration, is shown in Figure 8a, with the corresponding EDS spectrum in Figure 8b. The pronounced cracks, which can be seen extending into the mortar matrix and are not filled with alkali–silica gel, can be associated with dehydration of the gel.

The intensity of the alkaline attack on the flint particles is demonstrated by the BSE-images shown in Figure 9a and 9b. The BSE image in Figure 9a shows two aggregate particles: flint, on the left-hand side of the image, and inert aggregate, on the right-hand side. In contrast to the previous case, where the flint was only partially decomposed, the dissolution appears more advanced, and the whole flint particle is extensively etched (this is in fact localized dissolution of the unstable phase of the flint, i.e. the silica cement). The dissolution product is a lime-alkali-silica gel. Figure 9b shows the morphology of the gel surrounding a flint particle, with the corresponding EDS spectrum in Figure 9c.

Diatomite aggregate (D, D+IA)

The final set of investigated samples were the mortar bars containing diatomite aggregate. A large amount of lime–alkali–silica gel was observed in these samples, too, usually filling in all the voids, cracks and pores inside the specimen. In the BSE image shown in Figure

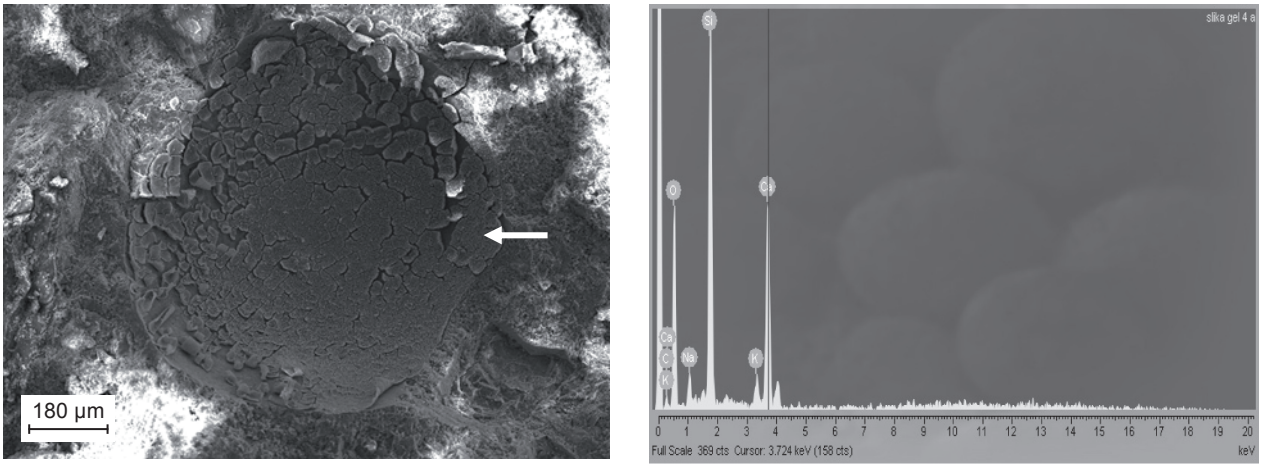

a) b)

Figure 5. (a) BSE image of an air void in the pure flint aggregate, filled with a lime-alkali-silica gel; (b) EDS spectrum of the gel (the analyzed point is marked by an arrow).

10a a uniform reaction rim running along the edge of the diatomite particle can be seen. This rim can be divided into three parts. The inner part of the rim is characterised by dense amorphous lime–alkali–silica gel, having a relatively light appearance and a thickness of less than 5 μm. The middle part of the rim has a porous radially-orientated structure, with a relatively dark appearance. It is concluded by a thin but dense layer, which makes up the outer part of the rim. The elemental composition of the layers across the rim is shown in Figures 10b, 10c, and 10d. The morphology of the reaction products on the fractured surface is shown, together with the corresponding EDS spectrum, in Figures 11a and b.

The (D+IA) mortar bar samples had the largest amount of lime–alkali–silica gel, which was concentrated in veins approximately 10-30 μm thick, spread all

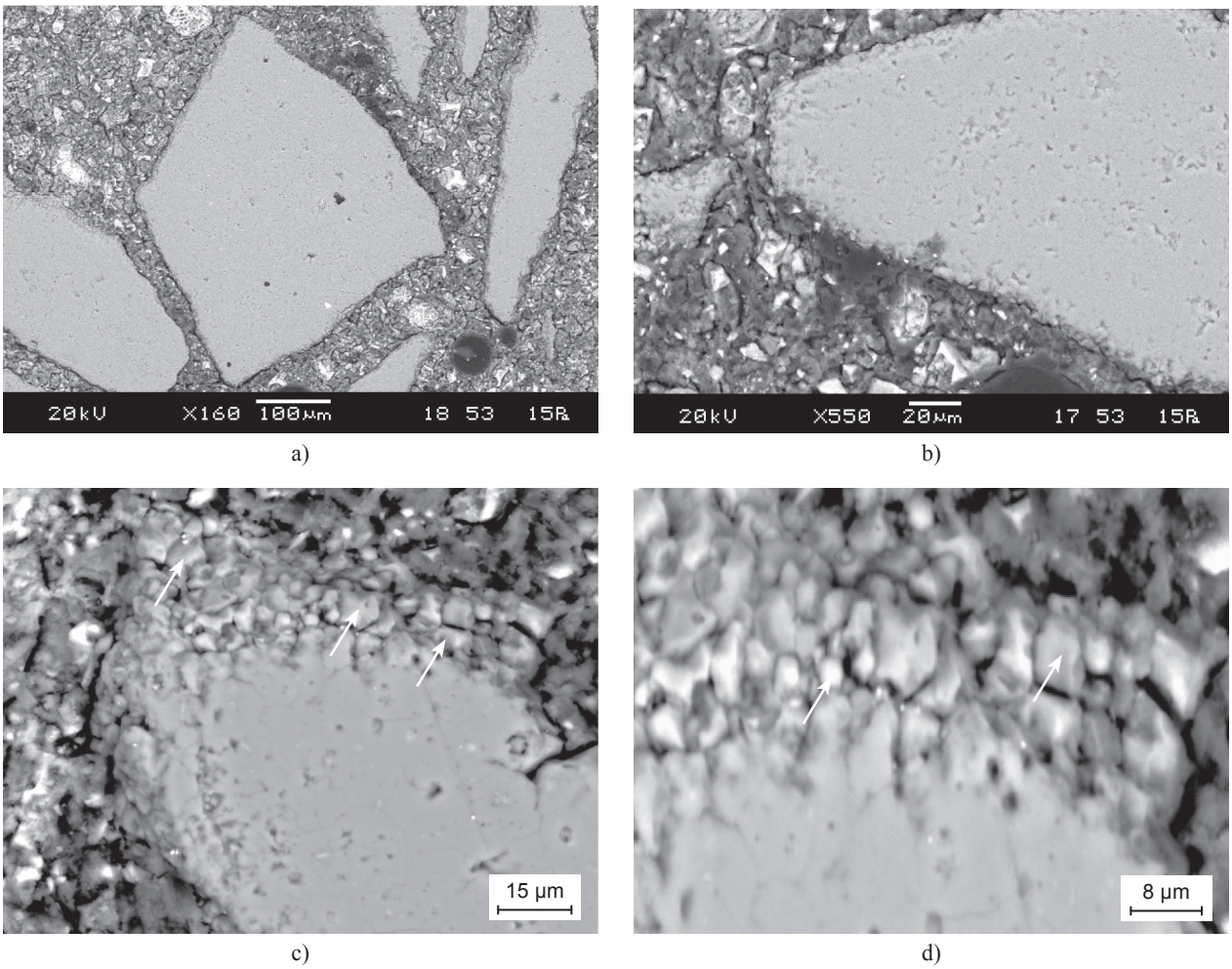

a) b) c) d)

Figure 6. BSE images of (a) original flint grains, (b) the same grains at a higher magnification, (c) a partly dissolved flint grain, and (d) the same grain at a higher magnification (the subgrains are marked by arrows).

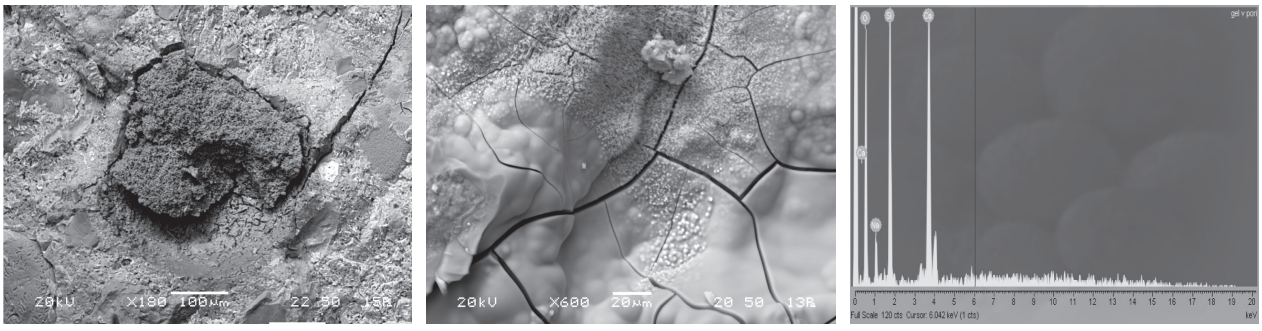

a) b) c)

Figure 7. (a) BSE image of the fractured surface of a partly dissolved flint particle, (b) the morphology of the reaction products, (c) EDS spectrum of the gel.

over the sample. An example of such a lime–alkali–silica gel vein, which passes close to an inert quartz grain, is shown in Figure 12. This vein shows discontinuities in the form of transverse cracks due to dehydration of the gel. Several cracks run from the gel into the aggregate particle, which could mean that the reaction was so severe that even non-reacting quartz particles can be broken along preferential paths of conchoidal fracturing. Similar findings regarding inert aggregate have been made by and Laing et al. [30], and by Nixon et al. [39].

Distribution of alkalis, SiO_2 and CaO content over the alkali-silica reaction rim

In order to determine the distribution of alkali, SiO_2 and CaO content over the alkali-silica reaction rim, linear scans were performed on the polished surfaces of the mortar bars. In all the aggregate samples a similar distribution of the elements was found, with Ca ions diffusing into the silica grains and Si ions diffusing in the opposite direction, i.e. into the cement matrix.

The results of a typical linear scan performed on the 5 % flint aggregate (F+IA) are shown in Figure 13. These results reveal that the highest concentration of Ca ions occurs in the middle of the reaction rim, with a decreasing trend towards the silica aggregate. On the other hand, the concentration of Si ions decreases from the SiO_2 matrix toward the cement paste. On average, the concentration of K and Na ions is less then 1 at. %, with a slight enrichment being evident at the rim's point of contact with the aggregate. The standard deviation of the atomic concentrations measured at each point did not exceed 2 %.

CONCLUSIONS

On the basis of the results of the experimental investigation, the following conclusions can be drawn:

1. All the investigated aggregates showed ASR, which produced Ca-rich, i.e. lime–alkali–silica gels. No pure alkali–silica gels were observed. The CaO/SiO_2 ratio

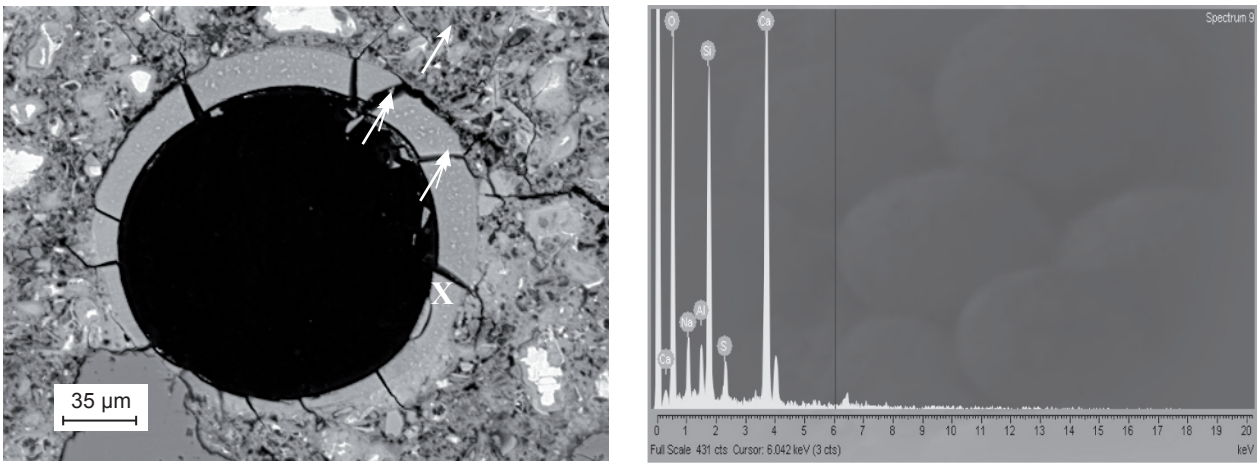

a) b)

Figure 8. (a) BSE image of an air void lined with lime-alkali-silica gel in the F + IA sample (the cracks propagating from the lime-alkali-silica gel into the mortar matrix are marked by arrows); (b) EDS spectrum of the gel (the analyzed point is marked by a cross).

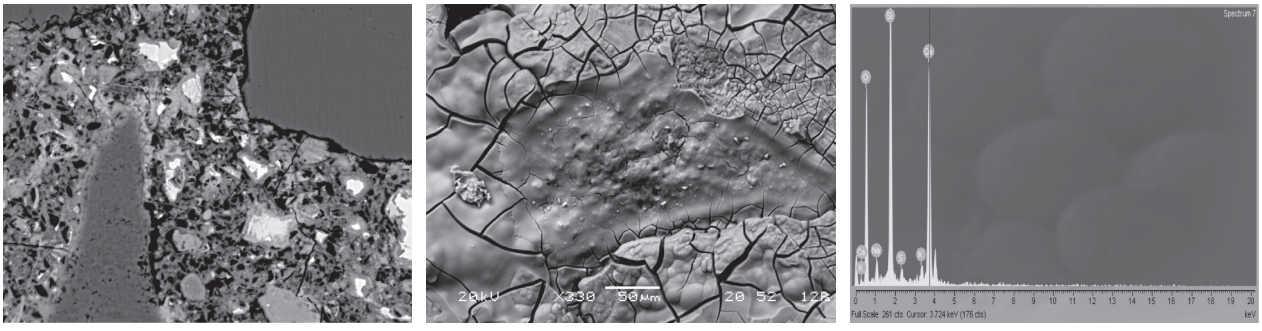

a) b) c)

Figure 9. (a) BSE image showing an extensively etched flint particle in the F+IA sample (left), whereas the inert aggregate (right) has not been affected; (b) BSE image of the fractured surface, showing the morphology of the reaction products; (c) EDS spectrum of the gel.

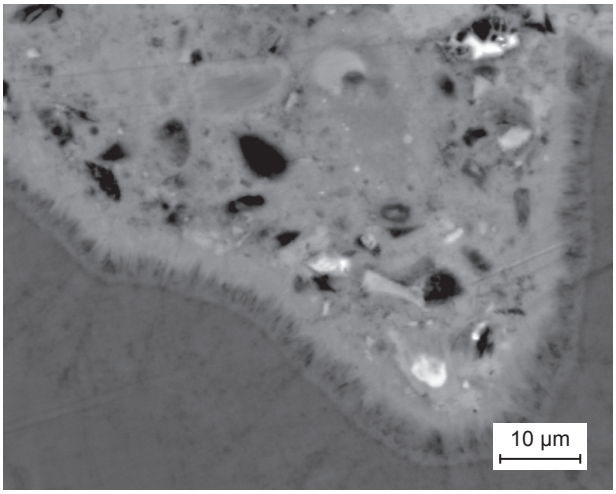

a)

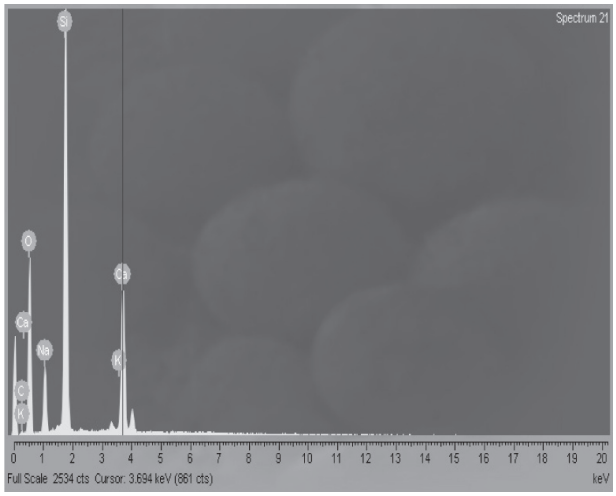

b)

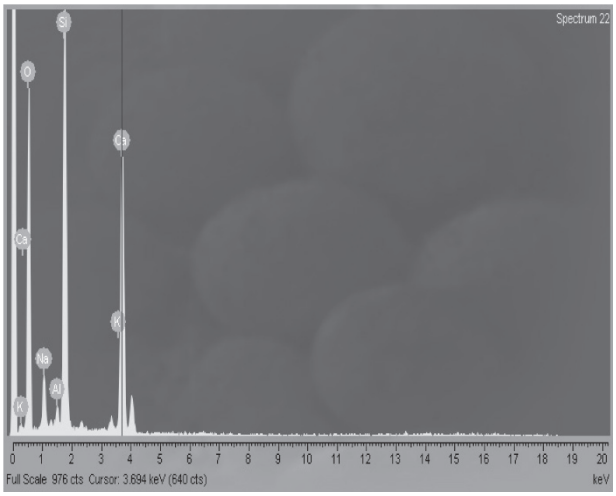

c)

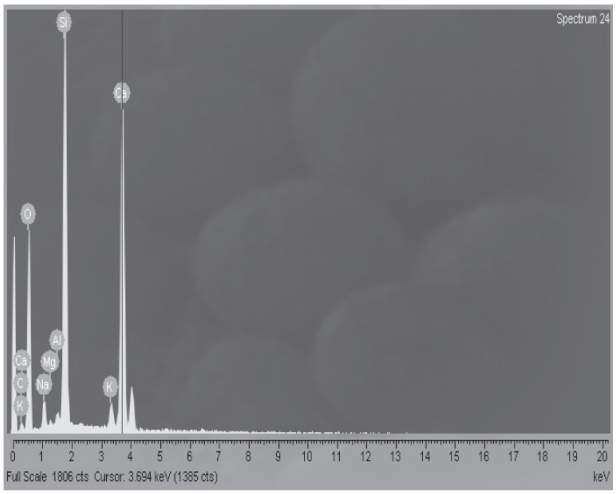

d)

Figure 10. (a) BSE image of a uniform alkali-silica reaction rim which has formed on the surface of a diatomite particle; (b) EDS spectrum of the inner part of the rim, (c) EDS spectrum of the middle part, (d) EDS spectrum of the outer part.

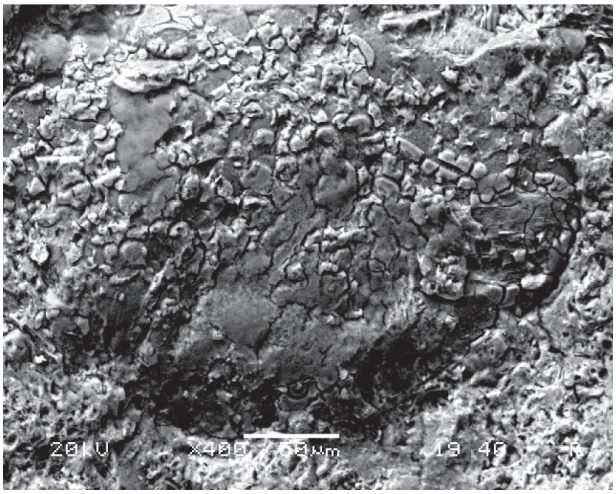

a)

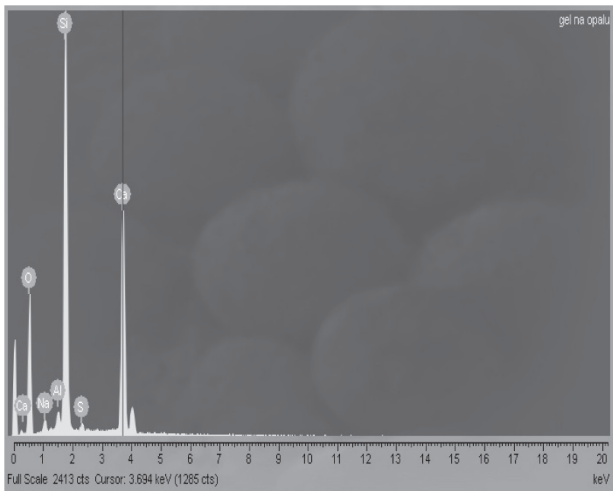

b)

Figure 11. (a) BSE image showing the morphology of the reaction products on the fractured surface of a diatomite particle; (b) EDS spectrum of the gel.

in the gels was between 0.3 and 1.6. The chemical composition of these gels was not influenced by the type and degree of crystallinity of the silica aggregate. Even in the large reactive grains, calcium predominated over potassium and sodium in the produced gel.

2. The measured expansion of the mortar bars correlated well with the degree of crystallinity of the different silica aggregates, expressed by means of a CI-index, particularly if the pessimum effect for flint and diatomite is taken into account. In the case of the mortar bars, which contained 5 % aggregate (F or D) and 95 % inert material, a significant linear expansion of approximately 0.56 % was observed in the case of the flint aggregate, and approximately 0.24 % in the case of the diatomite. No significant expansion was observed in the case of the quartz aggregate.
3. In the case of the F+IA and D+IA mortar bars, the measured expansion can be justifiably associated with large amounts of lime-alkali-silica gel and the appearance of microcracks, which occur in both the cement paste and in the grains of reactive aggregate, and, due to the severity of the reaction, sometimes even in the grains of the inert aggregate. The cracks are sometimes filled with gel. During later cycles of alkaline attack the unfilled cracks could provide open paths for the flow of alkaline solutions and swelling due to newly-formed alkali–silica gels. This means that study of the nature of cracks occurring inside experimental mortar bars could be very useful for the prediction of the long-term chemical and mechanical stability of mortars containing reactive aggregates.
4. The observed distribution of alkali, SiO_2 and CaO content over the lime–alkali–silica rim showed that the highest concentration of Ca ions was in the middle of the reaction rim, with a decreasing trend towards the silica aggregate. On the other hand, the concentration of Na and K ions amounted on average to only about 1.0 at. %, and was highest at the rim's point of contact with the aggregate. The high observed content of Ca in the gels, together with a very low content of alkalis, shows that, in the authors' opinion, Ca undoubtedly enters the grains together with the alkalis, and it is incorrect to think that it enters the grains as a secondary cation which would later partially replace the alkalis.

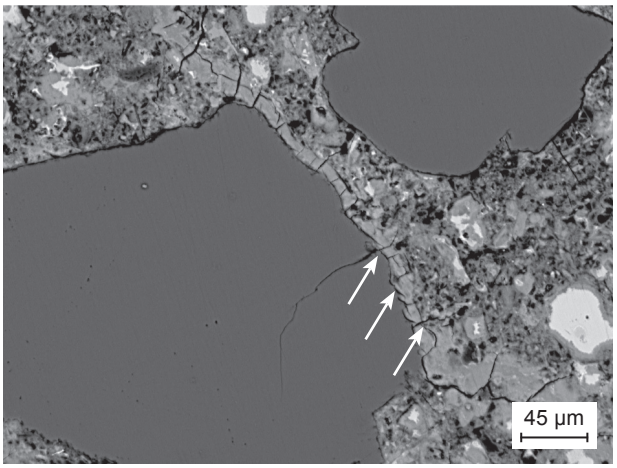

Figure 12. BSE image of a lime-alkali-silica gel vein in the D+IA sample. The crack in the aggregate grain is associated with the cracks observed in the lime-alkali-silica gel vein.

Acknowledgement

The extensive help of Peter Sheppard in the linguistic editing and preparation of this paper is hereby gratefully acknowledged.

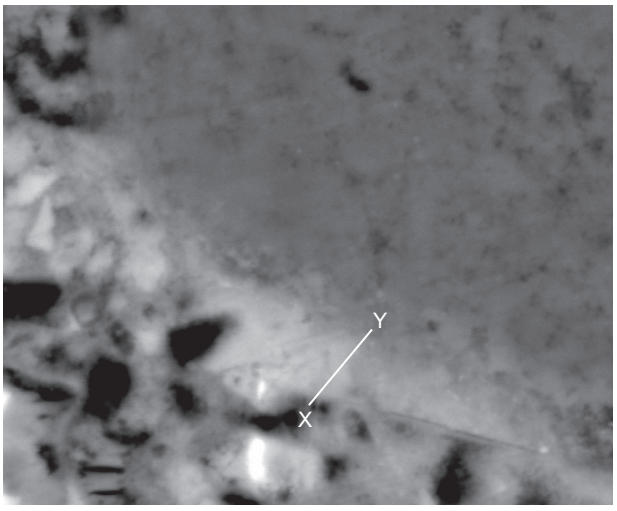

a)

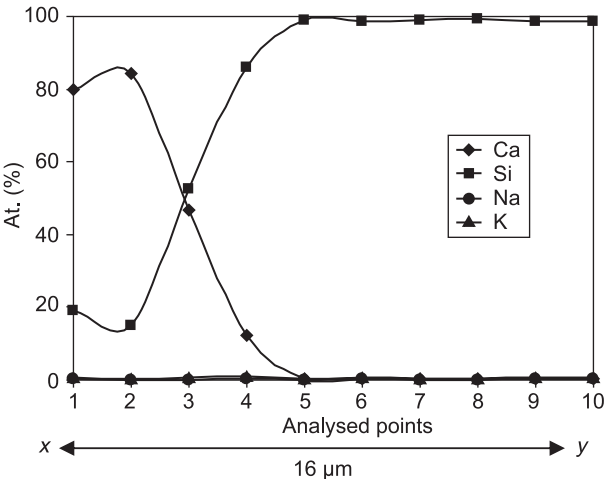

b)

Figure 13. (a) BSE image of a lime-alkali-silica reaction rim around a flint particle. Ten EDS line analyses from the outer part of the reaction rim towards the centre of the particle were performed, (b) scan profiles for the Si, Ca, Na and K atoms.

References

1. Robie R. A., Hemingway B. S., Fischer R.: U.S. Geol. Surv. Bull. p.1452 (1978).
2. Grattan-Bellew P. E. in: Proc. of the 9th International Conference on Alkali-Aggregate Reaction, pp. 383-394, Ed. A. B. Poole, The Concrete Society, London, 1992.
3. Broekmans M. A. T. M. in: Proc. of the 7th Euroseminar on Microscopy Applied to Building Materials, pp. 155-170, Eds. H. S. Pietersen, J. A. Larbi and H. H. A. Janssen, Delft, 1999.
4. Wakizaka Y., Moriya S., Kawano H., Ichikawa K. in: Proc. of the 8th International Conference on Alkali-Aggregate Reaction, Kyoto, pp. 519-524, Eds. K. Okada, S. Nishibayashi, M. Kawamura, Elsevier Applied Science, London & New York, 1989.
5. Deer W.A, Howie R.A., Zussman J.: An introduction to the rock-forming minerals, 2nd edition, Longman Scientific & Technical, Harlow, UK 1992.
6. Dove P. M. & Rimstidt J. D. in: Silica. Reviews in Mineralogy, pp.145-156, Eds. P. J. Heaney, C. T. Prewitt, G. V. Gibbs.
7. Murata K. J. & Norman M. B.: Am. J. Sci. *276*, 1120 (1976).
8. Katayama T. & Futagawa T.: Proc. of the 8th International Conference on Alkali-Aggregate Reaction, Kyoto, pp. 525-530, Eds. K. Okada, S. Nishibayashi, M. Kawamura, Elsevier Applied Science, London & New York, 1989.
9. Katayama T. in: Proc. of the East Asia Alkali-Aggregate Reaction Seminar, Supplementary papers, pp. A 45-59, Eds. S. Nishibayashi and M. Kawamura, Tottori, Japan, 1997.
10. Morino K. in: Proc. of the 8th International Conference on Alkali-Aggregate Reaction, Kyoto, pp. 501-506, Eds. K. Okada, S. Nishibayashi, M. Kawamura, Elsevier Applied Science, London & New York, 1989.
11. Powers T. C. & Steinour H. H.: J. Am. Concr. Inst. *26*, 6, (1955).
12. Wang H. &. Gillott J. E: Cem. Concr. Res. *21*, 4 (1991).
13. Chatterji S. in: Proc. of the 8th International Conference on Alkali-Aggregate Reaction, Kyoto, pp. 101-105, Eds. K. Okada, S. Nishibayashi, M. Kawamura. Elsevier Applied Science, London & New York, 1989.
14. Born M.: Z. Phys. *1*, 45 (1920).
15. Dogonadze R. R. & Kornyshev A. A.: J. Chem. Soc., London, Faraday Trans. II 70 (1974).
16. Rashin A. A. & Honig B.: J. Phys. Chem. *65*, 89 (1985).
17. Groves G. W. & Zhang X.: Cem. Concr. Res. *22*, 20 (1990).
18. Brouxel M.: Cem. Concr. Res. *25*, 23 (1993).
19. Thomas M. D. A.: *Materials Science of Concrete: Special Volume*, The Sidney Diamond Symposium, pp. 325-337, Eds. M.D. Cohen, S. Mindness, J. Skalny, The American Ceramic Society, Westerville, Ohio, 1998.
20. Kawamura R. A., Arano N., Terashima T. in: Materials Science of Concrete: Special Volume, The Sidney Diamond Symposium, pp. 261-276, Eds. M.D. Cohen et al., The American Ceramic Society, Westerville, Ohio, 1998.
21. Diamond S.: Proc. of the 11th International Conference on Alkali-Aggregate Reaction in Concrete, pp. 31-40, Eds. M. A. Berube, B. Fournier, B. Durand, Quebec City, Université Laval, Sainte-Foy, Quebec, 2000.
22. Prezzi M., Monteiro P. J. M., Sposito G.: ACI Mater. J. *94*, 1 (1997).
23. Knudsen T. & Thaulow N.: Cem. Concr. Res. *5*, 5 (1975).
24. Kurtis K. E., Monteiro P. J. M, Brown J. T., Meyer-Ilse W. Cem. Concr. Res. *28*, 3 (1998).
25. Lombardi J., Perruchot A, Massard P., Larive C. in: Proc. of the 10th International Conference on Alkali-Aggregate Reaction, pp. 934- 941, Ed. A. Shayan, Melbourne, 1998.
26. Davies G. & Oberholster R. E.: Cem. Concr. Res. *18*, 4 (1988).
27. Furnier B. & Berube M. A.: Cem. Concr. Res. *21*, 5 (1991).
28. Monteiro P. J. M., Wang K., Sposito G., dos Santos M. C., de Andrade W.P.: Cem. Concr. Res. *27*, 12 (1997).
29. Way S. J & Shayan A.: Cem. Concr. Res. *22*, 5 (1992).
30. Laing S. V., Scrivner K. L., Pratt P. L. in: Proc. of the 9th International Conference on Alkali-Aggregate Reaction, London, pp. 579-586, Ed. A.B. Poole, London, The Concrete Society, London, 1992.
31. Katayama T. & Bragg D. J.: Proc. of the 10th International Conference on Alkali-Aggregate Reaction, pp. 243-250, Ed. A. Shayan, Melbourne, 1998.
32. Jones J. B. & Segnit E. R.: J. Geol. Soc. Austr. *34*, 18 (1971).
33. Ozol M. A. in: Proc. of the Symposium on Alkali-Aggregate Reaction, Preventive Measures, Reykjavik, Icelandic Building Research Institute, Publication No. 16, 1975.
34. Hobbs D. W.: Mag. Conc. Res. *30*, 105 (1978).
35. Regourd-Moranville M. in: Proc. of the 8th International Conference on Alkali-Aggregate Reaction, Kyoto, pp. 445-456, Eds. K. Okada, S. Nishibayashi, M. Kawamura, Elsevier Applied Science, London & New York, 1989.
36. Leeman A. & Holzer, L. in: Proc. of the 9th Euroseminar on Microscopy Applied to Building Materials, Trondheim, pp. 155-70, Eds. M. A. T. M. Broekmans, V. Jensen and B. Brattli, 2003.
37. Broekmans M. A. T. M. & Jansen J. B. H.: J. Geochem. Explor. *43*, 62 (1998).
38. Rivard P., Ollivier J.-P., Ballivy G.: Cem. Concr. Res. *32*, 8 (2002).
39. Nixon J. P., Page C. L., Hardcastle J., Canham I., Petiffer K. in: Proc. of the 8th International Conference on Alkali-Aggregate Reaction, Kyoto, pp. 29-134, Eds. K. Okada, S. Nishibayashi, M. Kawamura, Elsevier Applied Science, London & New York, 1989.